RSC Advances

ROYAL SOCIETY OF CHEMISTRY

www.rsc.org/advances

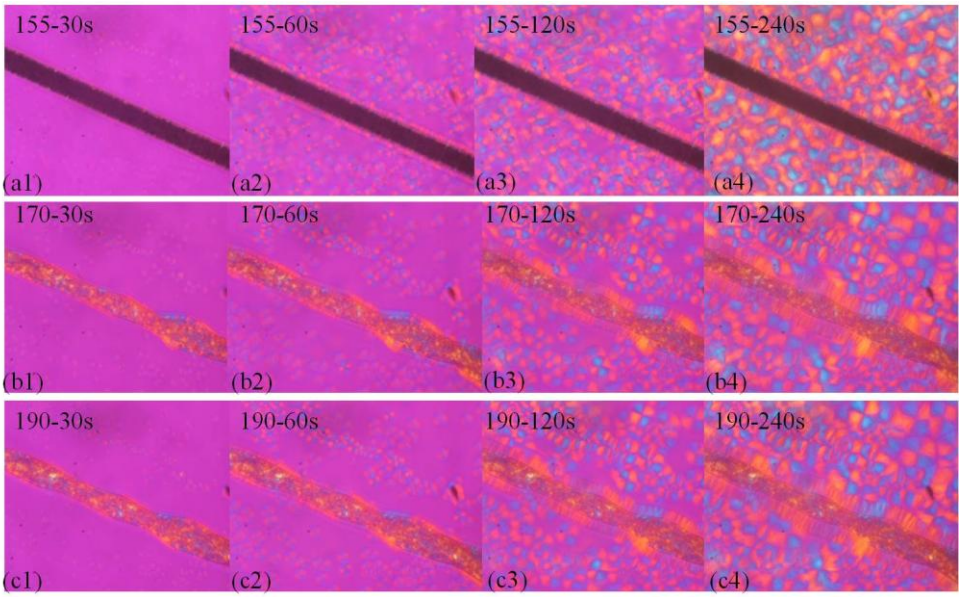

Transcrystalline structures for the first were observed at the interface of OBC/PP fiber, proving that the partially melted (170 ℃) and totally melted (190 ℃) PP fibers have stronger interactions with OBC than unmelted PP fibers does.

Cite this: DOI: 10.1039/c0xx00000x

www.rsc.org/xxxxxx

ARTICLE TYPE

Effect of melting temperature on interfacial interaction and mechanical properties of polypropylene (PP) fiber reinforced olefin block copolymers (OBCs)

Zhen Li, Yunjie Shi, Huili Liu,Feng Chen, Qin Zhang, Ke Wang, Qiang Fu*

Received (in XXX, XXX) Xth XXXXXXXXX 20XX, Accepted Xth XXXXXXXXX 20XX
DOI: 10.1039/b000000x

PP fiber reinforced olefin block copolymers (OBCs) were manufactured in the research. Chopped PP fibers were first compounded with OBCs at a fixed ratio in Haake mixer at 140 °C (lower than the melting point of PP fiber). The blends were then processed at three different temperatures, that is below (155 °C), around (170 °C) and above (190 °C) the melting temperature of the fibers. The three specimens displayed totally different mechanical properties according to the following sequence: 170 °C >190 °C >155 °C. To give an insight to the phenomenon, the structure-property relationships were fully investigated. It was found that when the blends were processed at 155 °C, the fibers kept the high strength and modulus yet losing the interaction with the matrix, displaying poor mechanical properties. At higher temperature at 190 °C, the fiber obtained strong interaction with OBCs. But the reinforcing effect was not satisfactory because the melted fibers lost the original modulus. When the blends were injection molded at 170 °C, the fibers were in partially melted state with strong interaction with the matrix and relatively high strength and modulus. Therefore the composites showed best mechanical performance. The article proves that fiber strength and interfacial bonding are the two factors that determined the final properties in fiber reinforced composites. Besides, it is suggested that the interfacial interaction could be improved via controlling the melting state instead of complex surface treatment of the fibers.

1. Introduction

Thermoplastic elastomers (TPEs) have been widely used in many fields due to their easily compounded characterics using traditional thermoplastic processing methods. Natural and synthetic rubbers are giving way to TPEs including styrenic block copolymers, polyurethanes, thermoplastic elastomer blends, and polyolefin elastomers and so forth.[1,2] Recently, the Dow Chemical Company synthesized olefin block copolymers (OBCs, INFUSE™) using novel chain shuttling technology.[3,4] The multi-block copolymers consist of crystallizable ethylene-octene blocks (hard blocks) with low octene concentration, alternating with amorphous ethylene-octene blocks (soft blocks) with high comonomer content. By controlling the concentration of chain shuttling agent, the length of hard and soft blocks can be regulated. [5-7]

Compared to other polyolefin elastomers like random ethylene-octene copolymers, the special blocky structure of OBCs imparts higher crystallinity while keeping better elastic and compression set properties at high temperature. Besides, they also exhibit improved abrasion resistance and faster cycle time.[5,6,8-10] Therefore, many researchers are involved to study the structure-property relationship of OBCs.[11-22] It is demonstrated the crystallization and mesophase separation morphology is dependent on chain structure like ΔC8 (the difference of octene content between the soft and hard blocks) as well as the length and constitution of the two blocks. For instance, Liu et al. found that OBC with higher ΔC8 exhibits mesophase separation and the fibrils-like crystalline lamellae in OBC with lower ΔC8 are dispersed in the amorphous matrix, while the lamellae in OBC with higher ΔC8 are confined in isolated meso-domains.[11] That may explain the different mechanical properties for the two OBCs. Zuo et al.[9,13] reported OBC synthesized with shuttling agent had shorter block length and it behaved more like random ethylene-octene copolymers. But its mechanical recoverability was poorer than the OBC with longer block length.

Based on the above, it can be concluded that the structure-property relationships are well established despite the relatively complex block structures. However, like other TPEs, the sole use of OBCs is restricted for load bearings due to the poor mechanical properties like low strain modulus and poor dimensional stability.[23] Usually second component is incorporated into the elastomers to realize the reinforcement to overcome the issue.[24] Tong et al. prepared OBC/organically modified montmorillonite (OMMT) nanocomposites with different dispersion states of clay.[25,26] The collapsed OMMT exhibited stronger nucleation ability on crystallization of OBC

Table 1 Characteristics of the OBC materials.

Sample code	Brand	Density (g/cm3)	Octene content(%)	Mw	Soft segment(%)	Hard segment(%)	MI (g/10min)	Tm(℃)
OBC	9530	0.888	10.4	78640	65	35	5	123

Table 2. Technical specifications of Innegra S

Parameter/properties	Value
Colour	white
Weight per Unit Length (denier)	625
Filaments per tow (count)	50
Ultimate Tensile Strength (MPa)	667
Tensile Modulus (MPa)	14828
Elongation at Break (%)	9.5
Creep @ 20% UTS	3.2
Diameter (μm)	38-42
Dielectric Constant	2.2

than intercalated OMMT, leading to different hierarchical and mechanical properties. Regrettably, the reinforcing effect was not so obvious as expected. If the goal is mechanical properties oriented, short fibers are considered to reinforce the matrix for the good strength and stiffness at a relative low fraction of fibers.[23,27-39] Among most of the fiber reinforced composites, surface modifications of the short fibers like aramid fiber or carbon fiber aiming at improving the adhesion between fiber and matrix is necessary.[28,31-33] Whatever the treatment process, it's always time-consuming and costly.

Previous study had proved that the soft segment of OBCs is expected to be partially miscible with isotactic polypropylene (iPP).[40,41] Besides, epitaxial crystallization even took place at the interface of olefin block OBC on uniaxially oriented iPP, which can improve adhesion, compatibility and mechanical properties in polymer blends.[17,42-44] Therefore, it is of interest to determine whether good interface adhesion can be achieved utilizing the partial compatibility or epitaxial crystallization between OBCs and the fillers via different melting state of PP fibers. In this article OBCs was reinforced by PP fiber and the interfacial adhesion was regulated through different process temperatures instead of complex fiber treatment process.

2. Materials and Methods

2.1 Materials

OBC, synthesized by chain-shuttling technology, was supplied by The Dow Chemical Company. The basic information on the material is shown in Table1, including density, octene content, molecular weight and soft and hard block proportion. PP fiber (trade name Innegra S) was purchased from Innegra Technologies. The detail specifications of the fiber are given in Table 2.

2.2 Preparation of composites

Before used, the chopped PP fibers were treated in boiling acetone for 2 h to remove the sizing agents and dust. Then they were dried in a vacuum oven at 40 °C for 24 h. The elastomers/PP fiber (90/10 w/w) composites were prepared in a Haake mixer (XSS-300, USA) at a temperature of 140°C and a rotor speed of 50 rpm for 10 min. After pelleting and drying, the blends were injected into a mold using the mini-injected machine (Haak MiniJet) with a barrel temperature of 155 °C，170 °C and

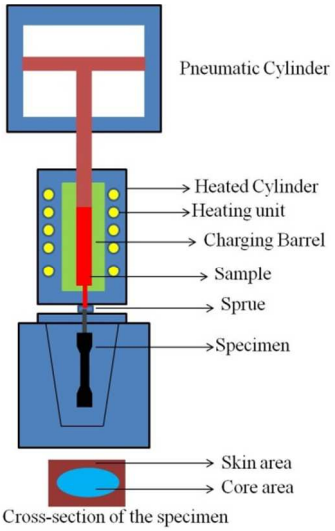

Fig.1 The sketch of the Haak MiniJet Machine

190 °C, respectively. The corresponding samples were noted as OBC-10PP-155, OBC-10PP-170 and OBC-10PP-190. Haak MiniJet machine is illustrated in Fig.1. Unlike the traditional injection molding machine, it is not equipped with screw. The samples are heated via the heating cylinder from out to inside. After the samples are plastified, the melt is injected into the mould relying on the pressure exerted by pneumatic cylinder. The obtained specimens also have skin-core structure like other injection-molded samples.

2.3 Tensile properties

A SANS universal testing machine (Shenzhen, China) was used to measure the tensile properties. Tensile measurements were made on dumbbell shape specimens 4 mm wide, 2 mm thick with a gauge length of 30 mm. A crosshead speed of 50 mm/min was applied to determine the tensile properties.

2.4 Interface

The interfacial crystallization morphologies of OBC and PP fiber were recorded by using polarized light microscopy (PLM) equipped with a hot-stage facility. The OBC thin film was first heated to 190 °C to erase the possible effect of thermal history and then cooled to 140 °C. After the fiber was introduced, the OBC/fiber composites were subsequently moved to another hot plate to crystallize isothermally. The composites were heated to 155 °C and then cooled at a rate of 100 °C /min for isothermal crystallization at 114 °C. After observation, the composites were reheated to 170 °C and 190 °C to repeat the same process, respectively. The crystallization morphology of the sample was recorded by taking photographs with a digital camera at a constant time intervals.

2.5 Differential scanning calorimetry (DSC) measurements

A differential scanning calorimeter (Perkin-Elmer pyris-1 DSC) with nitrogen as the purge gas was applied to study the melting behavior of PP fiber. The mass of tested sample was about 5 mg. In addition, the melting behavior of the samples taken from the skin and core area of all the tensile specimens was also characterized. They were directly heated from 30 °C to 200 °C with a rate of 10 °C/min and then cooled to 50 °C at the rate of 10 °C/min.

2.6 Rheological analysis

The melt rheology of OBC/PP fiber composites was measured in a strain-controlled dynamic rheometer Bohlin Gemini 2000, Malvern, British). For the measurement, disk-like samples obtained from the Haake mixer machine were used with diameters of 25 mm and thickness of 2 mm. The testing temperatures were controlled at 155 °C, 170 °C and 190 °C respectively, similar to that of the mini-injection molding process. To ensure a linear viscoelastic response, the strain amplitude was set as 1% with the frequency sweep was performed in the range of 0.06-628rad/s.

2.7 Scanning electron microscope (SEM)

The scanning electron microscopy (SEM) experiments were performed using an FEI Inspect F SEM instrument with an acceleration voltage of 20 kV. Surface of the raw PP fiber was directly observed after sputter-coated with gold powder. For morphological observations the composites, samples were firstly cryo-fractured in liquid nitrogen parallel and vertical to the shear flow direction, respectively. Then they were etched chemically in xylene at 80 °C for 20 min, followed by washing and drying.

2.8 Polarized Fourier-transform infrared

Measurements were carried out on a Thermo Nicolet FTIR spectrometer at a resolution of 4 cm^{-1} with an accumulation of 64 scans in reflection mode. Polarization of the beam was done by rotating a ZnSe polarizer. Films with thickness ca 30μm were cut from the skin and core areas of the tensile specimens parallel to flow direction. They were put perpendicular to the FTIR beam with a vertical machine and horizontal transverse direction. The measurements were performed with radiation polarized in the machine and transverse directions, respectively.

3 Results

3.1 Characterization of PP fibers

The thermal analysis of PP fibers was carried out by DSC. Fig. 2 (a) shows the melting thermograms of PP fibers. The fibers began to melt at 155.5 °C and two melting peaks at 160.3 °C and 172.2 °C were observed. Many research has reported that iPP fibers has a double melting endotherm.[45-48] To give one explanation, an article by Caldas indicates that the α-monoclinic crystalline morphology of iPP is generally composed of α1 and α2 form. The lower temperature peak (160 °C) and higher temperature peak (173 °C) are associated with melting of the α1 configuration and α2 configuration respectively. In oriented iPP fibers, the enthalpic transformation from α1 to α2 seems to be confined to occur in the temperature region between 156 °C and 163 °C and the double endotherm results from a superposition of an exotherm, resulting from the α1 to α2 conversion, onto the general melting endotherm.[48] Fig. 2(b) shows the SEM pictures of PP fibers at low and high magnifications, respectively. It can be seen that single fiber diameter is ca 40 μm and the surface is rather smooth.

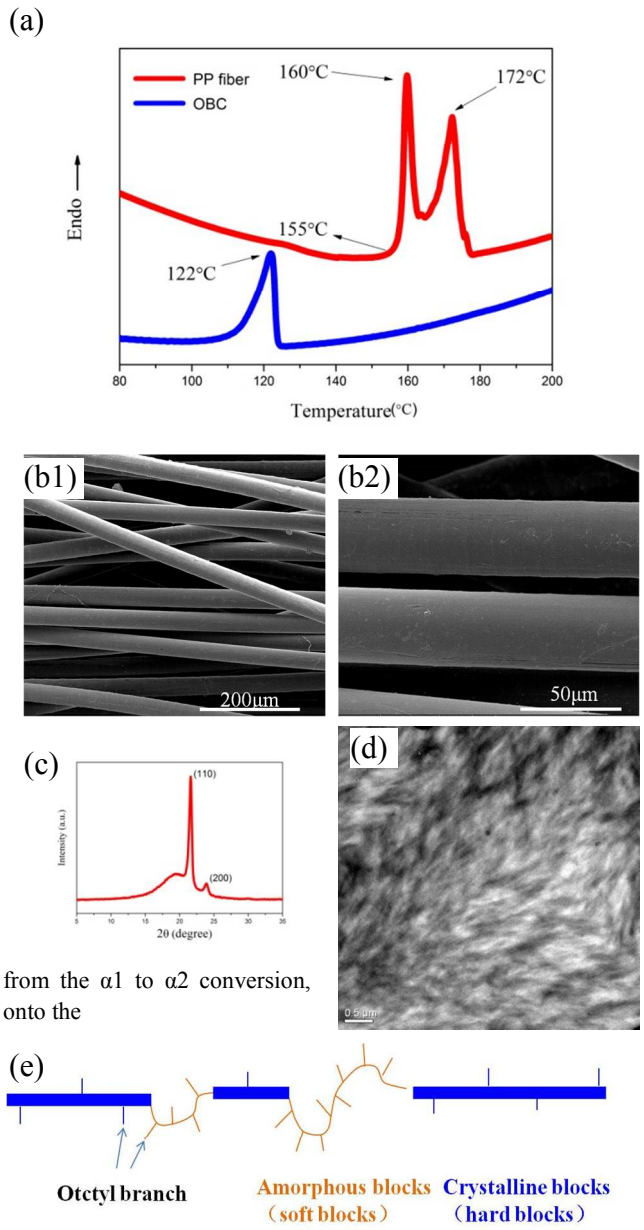

Fig. 2 (a) DSC curves of PP fibers and OBC elasomer (b) SEM pictures of pp fibers at low(b1) and high(b2) magnifications (c) WAXD pattern of OBC sample (d)TEM image of OBC(e) Sketch showing the structure of OBC

Fig.2 (e) shows the Alternating hard and soft segment structure of OBC and the Wide-angle X-ray diffraction (WAXD) and transmission electron microscopy (TEM) was introduced to characterize the OBC elastomer (Fig2 (c) and (d)). The OBC has a melting point around 122 °C. From the WXRD pattern, OBC exhibits two sharp diffraction peaks at 2 θ of 21.1° and 23.6°. They belong to the (110) and (200) reflections of orthorhombic

polyethylene (PE) crystals respectively. The hard blocks formed the PE crystals as is displayed in the TEM picture where the dark areas correspond to the crystalline domains.

3.2 Tensile properties

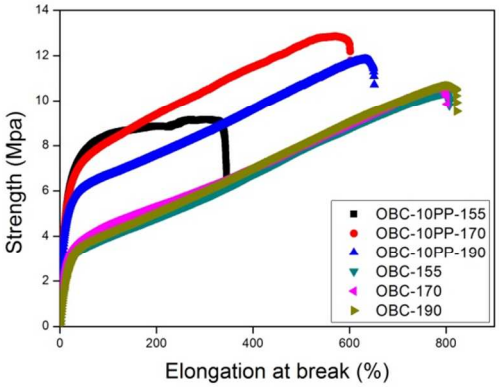

Fig. 3 Strain-stress curves of PP fiber reinforced composites mini-injection molded at different temperatures.

Table 3 mechanical properties of OBC and its composites

	Elongation at break(%)	300% Tensile strength (MPa)	Breaking strength (MPa)
OBC-155	765.1±42.74	5.9±0.83	10.1±0.72
OBC-170	783.8±32.92	6.1±0.71	10.24±0.78
OBC-190	775.6 ± 35.86	5.7±0.52	9.7±1.944
OBC-10PP-155	366.5 ± 38.40	9.1±0.73	8.81±0.22
OBC-10PP-170	595.1 ±5 8.39	10.4±1.35	12.7±0.47
OBC-10PP-190	668.2 ± 14.54	8.6±0.94	11.94±0.43

Fig. 3 shows the stress-strain curves of OBC/PP composites and table 3 summarizes the mechanical properties of the composites. It can be seen that tensile properties of neat OBCs keep stable regardless of the temperature changing. Besides, the incorporation of PP fibers exerts different effect on the mechanical behaviors at elevated temperatures. Firstly, when injected at 170 °C, the elastomer/fiber composites exhibit best tensile properties with balanced tensile strength and elasticity. At higher injected temperature, the tensile strength decrease somewhat but still better than neat OBCs. However, when the samples were prepared at 155 °C, the composites show undesirable properties with dramatically decreased elasticity and breaking strength. Therefore OBC-10PP-190 shows better mechanical properties than OBC-10PP-155 from overall point.

3.3 Interfacial interaction

The interface between matrix and fiber is one of critical factors that decide the final mechanical properties of polymer/fiber blends. Usually favorable interfacial adhesion is achieved to transfer load from matrix to fibers.[49] Transcrystalline (TC) is one of the hybrid crystalline structure, formed due to the high density of active nuclei on the fiber surface. It has been proved that the unique structure may be responsible for realizing effective interfacial adhesion.[50] Therefore, in this article TC was also introduced to help better understand the interaction between OBC and PP fibers. TC morphology is often induced where semicrystalline polymers served as matrix like polypropylene and polyethylene instead of elastomers.[50-52] The crystallizable ethylene-octene blocks (hard blocks) endows OBCs with relatively high crystallinity, making it possible to form elastomer/fiber transcrystalline. Here， OBC/PP fiber TC was firstly observed as is exhibited in Fig. 4.

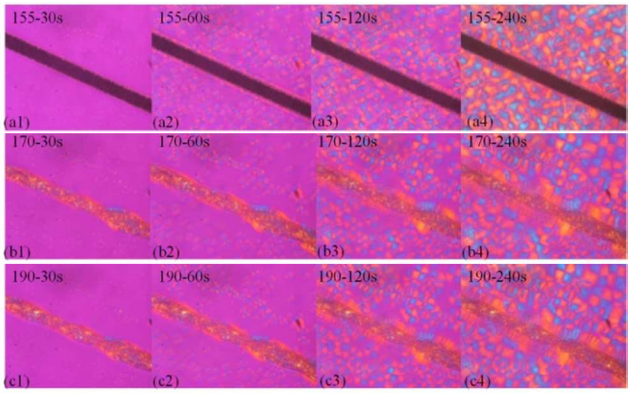

Fig. 4 Transcrystallization evolution at the interface of OBC and PP fibers. Isothermal crystallization was observed at 114 °C after cooling from different temperatures:(a1-a4) 155 °C (b1-b4) 170°C and (c1-c2) 190 °C

According to the three temperatures used in mini-injected process, the same temperatures were also used to get different initial fiber morphology before cool to crystallization temperature. It should be noted that at 170 °C, PP fiber was almost melted. The phenomenon is acceptable since the melting temperature may shift toward lower temperatures considering the fiber was in less constrained state. From Fig.4, it can be seen that all the three groups of samples show obvious transcrystalline structures and the TC layers reach to the maximum after 240s of isothermal crystallization. The evident difference lies in the thickness of TC layer. When the samples cooled from 170 °C and 190 °C, the TC layers are thicker than that cooled from 155 °C. To give a reasonable explanation, compatibility between matrix and different melting state of PP fiber should be fully considered. It has been found that the soft blocks of OBC are compatible with PP and the interface where OBC and PP molecules were inter-penetrated is likely to be the region for creating the nuclei.[16,22] When the samples cooled from 170 °C or 190 °C, some degree of molecular relaxation at the surface of the fiber made it easier for the OBC molecules to diffuse into the relaxed PP chains. So, both nuclei density and the probability of molecular attachment increased, forcing the crystal growth in one direction to form thicker TC structure when isothermal crystallizing at 114 °C. Whereas for the isothermal crystallizing samples cooled from 155 °C, PP molecules were confined in the ordered crystal lattice. So the comparably smooth fiber surface will simply act as a substrate for homoepitaxy due to lack of such chain relaxation and inter-diffusion. The relatively thinner TC layer indicates the interface interaction is weaker than the former two composites.

To further investigate the interfacial interactions, we used the solubility parameter (δ) difference from cohesive energy density (CED) parameter values of both polymers to estimate the Flory - Huggins interaction parameter χ： [53-57]

$$\chi = (\delta_A - \delta_B)^2 \ V_r/(RT) \quad (1)$$

$$V_r = [([M]_A V_A)([M]_B V_B)]^{1/2} \quad (2)$$

$$\delta = (CED)^{1/2} \quad (3)$$

$$CED = (\gamma/0.75)^{3/2} \quad (4)$$

Where V_r is the reference volume, an average volume of repeated units, R is the gas constant, and T is the temperature (K); $[M]_A$ and $[M]_B$ are the monomeric molecular weights of components A and B, respectively, and V_A and V_B are the specific volumes of components A and B; R is the gas constant, and T is the temperature (K); γ is the surface free energy (SFE), which can be calculated from the contact-angle measurement according to the equation.[53]

$$(1+\cos\theta)\gamma_l = 2[(\gamma_s^d\gamma_l^d)^{\frac{1}{2}} + (\gamma_s^p\gamma_l^p)^{\frac{1}{2}}]^{\frac{1}{2}} \quad (5)$$

$$\gamma = \gamma^d + \gamma^p \quad (6)$$

where γ is in mJ/m^2， CED is in $10^6 J/m^3$, δ is in $10^3\ J^{1/2}/m^3$.

In this study, the values of γ_{PP} and γ_{OBC} at 190 °C were by reference to literature [58] and we used the γ value of ethylene–octene copolymer (POE) to substitute OBC since they have similar structures. According to the literature, the dependence of SFE on temperature is linear and the temperature coefficient for PP was found to be 0.058 mJ/m^2 per degree.[59] Served as one novel olefinic elastomer, the temperature coefficient for OBC could not be found. Here we used the same value of PP for substitution, i.e. 0.058 mJ/m^2. Therefore, the γ value at 155°C, 170 °C and 190 °C can be obtained.

Because V_r and R are both temperature-independent constant, to simplify the calculation process we define $X=(R/V_r)\chi=(\delta_A-\delta_B)^2/T$. So X can represent the changing trend of χ (X is in 10^3 $J/(m^3K)$). The results are concluded in table 4

Table 4 the values of γ and X at different temperatures

Materials	γ(mJ/m²)			X(10^3J/(m^{3}K))		
	155 °C	170°C	190 °C	155°C	170°C	190 °C
PP	34.37*	22.86	21.7	86.53	7.58	7.46
OBC	19.53	18.66	17.5			

*Note: PP had turned into solid state at 155 °C, the γ value at 25 °C was used here.

From table 4, $X_{155}>X_{170}\approx X_{190}$, indicating that OBC-10PP-155 has poorer interfacial interaction than OBC-10PP-190 and OBC-10PP-190. It is understandable that at 155 °C, PP fiber was still in solid state and the constrained PP molecules got no chance to interfuse with OBC molecular chains, resulting poor miscibility and interaction. Whereas at 170 °C and 190 °C, the relaxed PP chains were more likely to entangle with OBC chains, thus enhance the interfacial bonding and displaying lower X values.

3.4 Thermal analysis

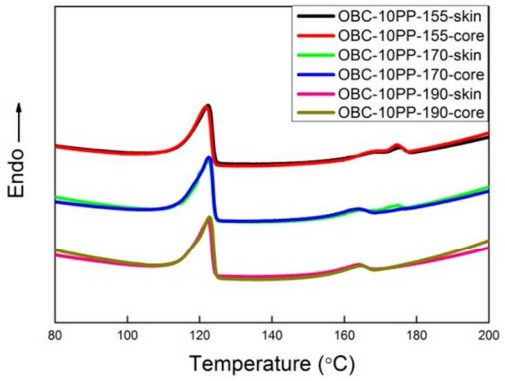

Fig. 5 DSC curves of skin and core area samples from mini-injection molded specimen at different temperatures

Fig .5 exhibits the first DSC heat thermograms of the samples cut from skin and core areas of the three injection-molded specimens. As is pointed out in Fig. 2 (a), the peaks around 122 °C belong to the melting point of the OBC matrix and they nearly changed regardless of the processing temperature. The fibers show two peaks in OBC-10PP-155, which is in accord with the former result since the fiber had not yet started to melt. The slight difference can be seen that the two peaks shift to higher temperatures compared with the result of neat PP fibers. It is because that the more constrained PP fiber in injection molded composites resulted in higher melting temperature than the neat loose PP fiber.[45] For OBC-10PP-190, only one melting peak at 164.1 °C is observed regardless of the sampling position, indicating the totally melting of the fibers throughout the specimens. Unexpectedly, OBC-10PP-170 show unique DSC patterns: the skin area exhibits two melting peaks like OBC-10PP-155 whereas the core area only has one similar to OBC-10PP-190. Compared with OBC-10PP-155, the lower peak of OBC-10PP-170 becomes more obvious and shift to lower temperature, which agrees with typical melting behavior of PP granules. In addition the appearance of higher melting peak proves that parts of the PP fibers are still in unmelted and oriented state. Yet PP fibers localized at the inner part of the specimen only show one melting peak. Based on the above, it can be deduced the fibers in skin zone were just partially melted and that in the core area were totally melted. The discrepancy may first arise from the different fiber constraint state in the charging barrel before injected. The skin and core area of the specimen result from the melt adjacent to the barrel and the melt in the middle of the barrel respectively. It can be easily understood that the samples adjacent to the barrel were in a more stressful field than that in the middle of the barrel, making it harder for the fiber molecules to relax for a limit time at 170 °C.[45] Although the heating was applied from the barrel wall to the inside, the more constraint fibers still kept its fiber morphology and exhibit partially melted characterisc. On the contrary, the blend pellets in the middle of the barrel were loosely distributed. Therefore the less confined PP fibers in the middle of the barrel were more likely to melt and finally reached to a totally melted state.

3.5 Rheology property

As shown in Fig.6 (a), the addition of PP fibers exerts a stronger effect on the rheology properties. The effect is more prominent at low angular frequency for elastic modulus. When tested at 155 °C, the PP fiber was unmelted and the rigid PP fiber molecular contributed to the highest elastic. Particularly, at 170 °C and 190 °C, the neat OBCs almost show the same elastic modulus. After blended with PP fibers, the composites tested at 170 °C exhibit more obvious reinforcing effect than that at 190 °C, which may be attributed to the oriented PP chains in the partially melted sample. Fig. 6(b) illustrates the plot of tan δ vs. angular frequency, which represents the damping characteristic of the composites. The plot reveals a considerable decrease after the incorporation of PP fibers. Special consideration should be paid that the damping behaviors are almost the same as the composites tested at 155 °C and 170 °C. Because part of the oriented PP molecules had already relaxed at 170 °C, better adhesion enhances the interaction between OBC and PP, which restricts the molecular mobility of the OBC chains in the melt and further

decreased tan δ value. That effect to some extent compensates the strength drop caused by PP molecular relaxation.

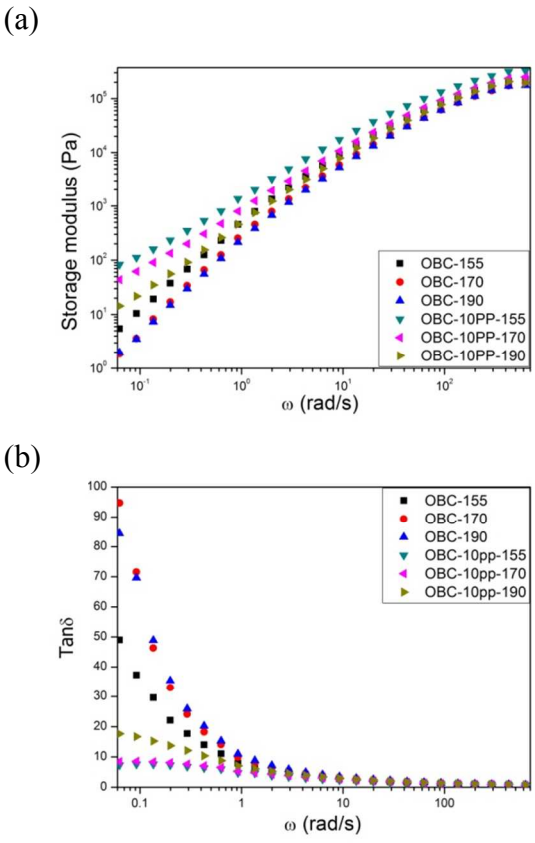

Fig.6 The storage modulus (a) and tan δ (b) vs. angular frequency for OBC/PP fiber composites at different temperature

3.6 Fiber morphology and orientation

Fig. 7 shows the SEM pictures of the cross-section of the injection molded specimens perpendicular to flow direction. The fibers in OBC-10PP-155 kept the original morphology across the whole cross-section and failed to melt at all. Although transcrystallinity appeared in the single fiber mode under mild conditions, the interfacial adhesion was still too weak to resist the swollen effect of xyene and clear debonding gaps appeared at the interface of fiber and matrix. That proved tiny voids may exist at matrix/fiber interface. Oppositely, when molded at 190 °C, PP fibers were totally melted and the molted PP transformed in more delicate structure of microfibers and no cracks at the surface of microfibers were observed. Normally when the fibers are heated to a temperature higher than 175 °C, the fibers would shrink and may form spherical or ellipsoidal particles. However, here in the cylinder of the mini-jet machine, the fibers were in a constrained state. Even when they were heated to 190 °C, the fibril structures were kept. During the injection process, the fibers were in the constraint state all the time. Due to the shear stretch effect, the fibers finally turn into more tiny microfibrils with several microns. Although they had the fibril morphology, the inside crystal structure of original PP fibers had been destructed and also the strength of the PP phase would decrease. For OBC-10PP-170, fibers in the skin area not completely kept the original morphology and the shape deformed to some extend when the injection pressure was imposed, exhibiting partially melting characteristic as proved by DSC test. Also, no obvious defects were observed at the interface of partially melted fi(a2) id matrix.

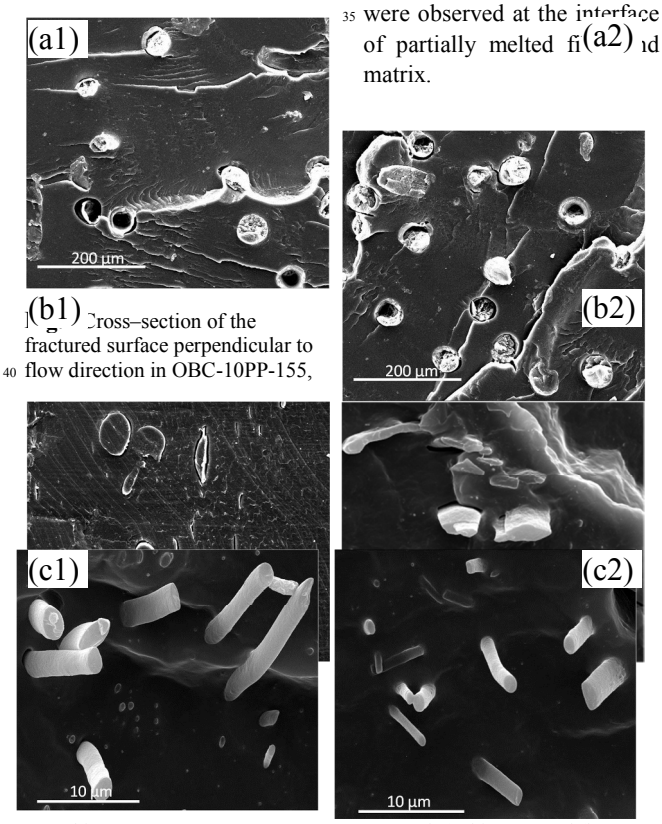

Cross–section of the fractured surface perpendicular to flow direction in OBC-10PP-155, (a1) skin area (a2) core area; OBC-10PP-170, (b1) skin area and (b2) core area; OBC-10PP-190, (c1) skin area (c2) core area

In the core area, PP fibers were totally melted and the morphology was similar to that in OBC-10PP-190 composites.

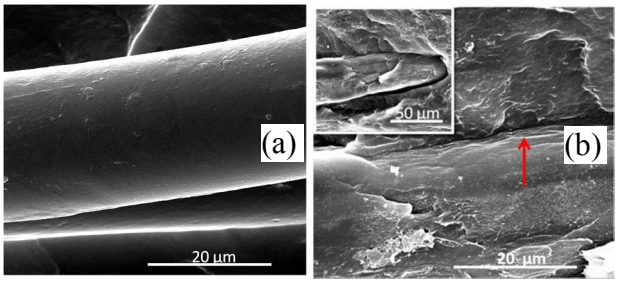

(c)

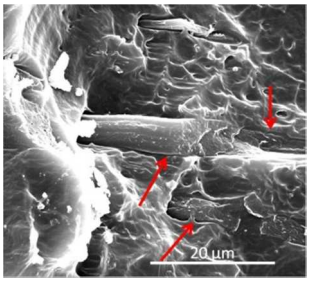

Fig.8 fracture surface of the skin regions parallel to flow direction in （a） OBC-10PP-155 （b） OBC-10PP-170 （c） OBC-10PP-190

Fig. 8 exhibits the fracture surface of the skin regions parallel to flow direction. Obviously in OBC-10PP-155, PP fibers were

pulled out from the matrix and the smooth surface indicated poor interfacial adhesion. For the partially melted fibers in OBC-10PP-170, the diameter of the fibers became larger than 50 μm with rougher surface due to molecular relaxation. The fiber was inserted into the matrix and no cracks appeared along the interface. For OBC-10PP-190, the subsize microfibrils and matrix show a blurred interface.

It has been reported that the soft segment of OBCs is expected to be partially miscible with the amorphous region of iPP[41]. Here, when the injection temperature (155°C) was below the melting point of PP, all the PP chains were confined in the crystal lattice of the solid fibers, showing poor miscibility with the OBC matrix. Although the fibers kept the original strength and modulus, OBC-10PP-155 still showed undesirable mechanical properties because of poor interactions. However for OBC-10PP-170 and OBC-10PP-190, whether PP fibers were partially melted or totally melted, The PP relaxed molecules were interfused with OBC chains and such kind of chain-entanglement dramatically enhances the miscibility between the matrix and PP phase, proved by the blurred interface. Therefore strong interfacial bonding would be achieved at the two temperatures. The results are in accord with the X values.

The orientation degree of polymers can help better understand their dispersion states and to calculate PP orientation function, the following formulas were used:

$$f = [(R-1)/(R+2)/[3\cos^2\alpha - 1]/2] \quad (7)$$

$$R = A_{\parallel} / A_{\perp} \quad (8)$$

Where A|| and A⊥ are the parallel and perpendicular absorbance, respectively, and α is the angle between the dipole moment vector and the local chain axis. Typical FTIR spectra machine and transverse directions for the composites are shown in Fig. 8 (a) and (b). The 841 cm^{-1} were observed to be associated with the PP crystalline phase and the 998 cm^{-1} was assigned to both crystalline and amorphous phases of PP. Here, the orientation function was calculated using 998 cm^{-1}, for which the value of α was taken as 18°.[60] The FTIR spectra indicate that the different molten state of PP fiber corresponds to different orientation behaviors. The orientation functions of PP in the composites are shown in Fig. 8 (c).PP in the core area failed to orient due to the absence of shear field. PP orientation in the skin area of the three samples differs a lot according to the following order: OBC-10PP-170>OBC-10PP-190>OBC-10PP-155.

To figure out the possible factor influencing the orientation, the complex viscosities for the samples tested at three different temperatures is shown in Fig. 10. Complex viscosity is a frequency-dependent viscosity function determined during forced harmonic oscillation of shear stress. It can reflect the processing fluidity of the melt to some extent. It is clear that, because of the solid PP fiber, the complex viscosity of OBC-10PP-155 is higher than the other two blends processed at 170 °C and 190 °C. The extremely high complex viscosity hindered the PP fibers to orient according to external shear field. Whereas for OBC-10PP-190, its complex viscosity was even lower than OBC-155, showing improved processability. Thus the liquid PP phase was more likely to orient along the shear field under the injection pressure. Although OBC-10PP-170 displayed higher complex viscosity than OBC-10PP-190, its orientation was supposed to be lower than the later one based on the above explanation. However it

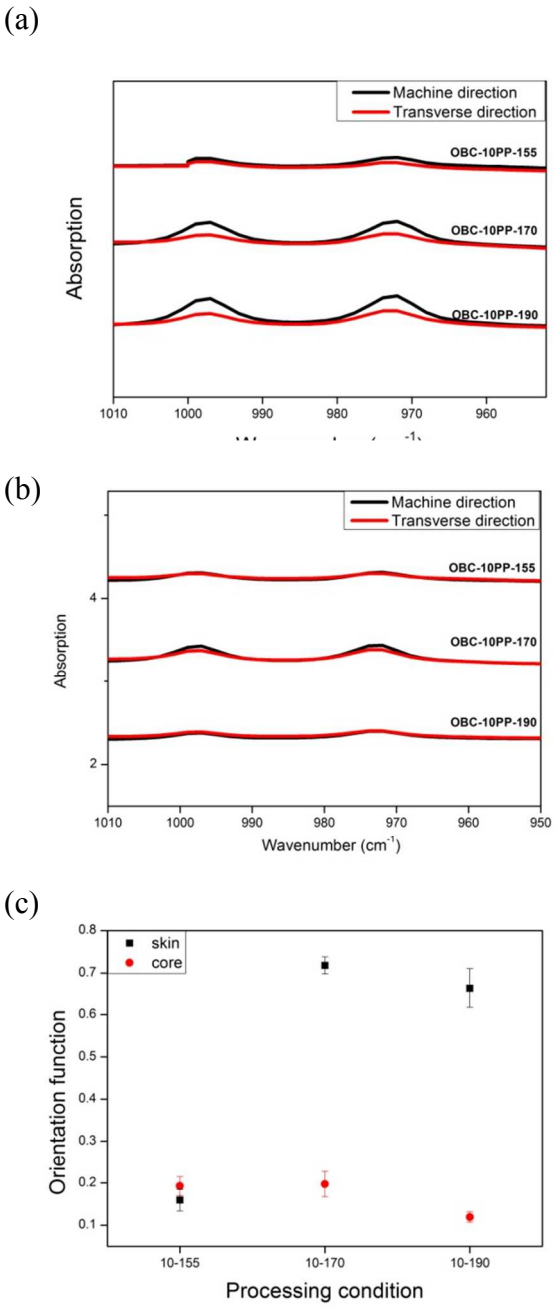

Fig.9 Polarized FTIR spectra of OBC-10PP-155, OBC-10PP-170 and OBC-10PP-190 in machine (SM) and transverse (ST) directions: (a) skin area and (b) core area; (c) The corresponding orientation function in the three composites

should be noted that in the skin layer of OBC-10PP-170, PP fibers were only partially melted and the PP molecule chains already kept a relatively high orientation degree before injection molding. After oriented along the shear field, the PP chains would exhibit higher orientation degree than OBC-10PP-190 with totally relaxed PP phase. The higher orientation function of the fibers with relatively high strength and modulus make OBC-10PP-170 own better mechanical properties than OBC-10PP-190,

of which the PP chains were fully disoriented and the strength and modulus of PP deceased dramatically

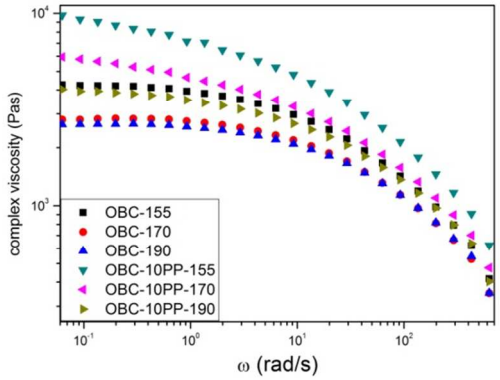

Fig.10 Complex viscosities for neat OBC and the composites tested at three different temperatures

Summarizing the above analysis, Fig.11 schematically illustrates the three different structures that decide the final properties, in which the skin areas are enlarged. For OBC10-PP-155, interactions between matrix and fibers are weak and the random distribution of PP fibers failed to effectively improve the OBC properties despite the fibers kept the original strength. Totally melted PP fibers in OBC-10PP-190 realized fully interacted molecules of the two polymers. However the totally disoriented fibers lost their original strength and modulus, the reinforcing effect was not satisfactory. OBC10-PP-170 obtains the balanced interfacial interaction and fiber strength. The totally melted fibers inside the specimen and partly melted fibers (the enlarge part in fig.11 (b)) outside guaranteed the entanglement of matrix and PP molecules and thus enhance the miscibility between the two polymers. Besides, the crystal structures in the partially melted fibers were retained, making them suitable to work as appreciably reinforcing skeleton with relatively high strength.

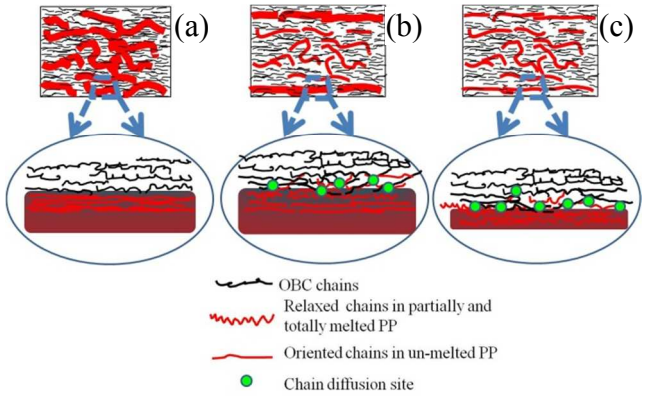

Fig.11 Structure models of composites injection molded at different temperatures (a) OBC-10PP-155 (b) OBC-10PP-170 (c) OBC-10PP-190

5 Conclusion

PP fiber reinforced OBCs were successfully prepared through internal mixing and mini-injection molding. Through differed injection temperatures, three PP fiber states namely unmelted, partially melted and totally melted were achieved (proved by DSC result). When processed at 170 °C, PP fibers were partially melted in the skin area whereas totally melted in the core area with more delicate morphology. The unique structure endows the composite with best tensile performance. OBC-10PP-155 and OBC-10PP-190 exhibited less prominent reinforcing effect either for poor interfacial adhesion or totally relaxed PP fiber. Two key factors: interfacial adhesion and PP fiber strength were fully characterized to explain the discrepancy. Particularly, when investigating the interfacial bonding, tanscrystalline (TC) structure was for the first time traced at OBC elastomer and PP fiber interface. The phenomenon was more pronounced with thicker TC layers when PP molecules were relaxed. This interesting result may need further investigation to fully explore the TC structures between elastomer and fibers. That may help better understand the interfacial interactions.

Acknowledgements

This work was supported by the National Natural Science Foundation of China (51121001 and 51210005) and the Special Funds for Major State Basic Research Projects of China (2011CB606006)

Notes and references

*College of Polymer Science and Engineering, State Key Laboratory of Polymer Materials Engineering, Sichuan University, Chengdu 610065, China. Fax: 0086-28-85405402, Tel: 028-85405402, Email: qiangfu@scu.edu.cn

1 Z. Z. Tong, J. Huang, B. Zhou, J. T. Xu, and Z. Q. Fan, *Macromol. Chem. Phys*., 2013, **214**, 605-616
2 F. Zuo, Y. Mao, X. Li, C. Burger and B. Hsiao, *Macromolecules*, 2011, **44**, 3670-3673
3 P. S., Chum and K. W. Swogger, *Prog. Polym. Sci.*, 2008, **33**, 797-819
4 D. J., Arriola, E. M. Carnahan, P. D. Hustad, R. L. Kuhlman and T. T. Wenzel, *Science*, 2006, **312**, 714-719
5 D. U. Khariwala, A. Taha, S. P. Chum, A. Hiltner and E. Baer, *Polymer,* 2008, **49**, 1365-1375
6 H. P. Wang, D. U. Khariwala, W. Cheung, S. P. Chum, A. Hiltner and E. Baer, *Macromolecules*, 2007, **40**, 2852-2862
7 H. E. Park and J. M. Dealy, *Macromolecules,* 2010, **43**, 6789-6799
8 C. Shan and L. G. Hazlitt, *Macromol. Symp.*, 2007 , **257**, 80-93
9 H. P. Wang, S. P. Chum, A. Hiltner and E. Baer, *J. Polym. Sci. Part B:Polym. Phys*., 2009, **47**, 1313-1330
10 H. P. Wang, S. P. Chum, A. Hiltner and E. Baer, *J. Appl. Polym. Sci.*, 2009, **113**, 3236-3244
11 G. Liu, Y. Guan, T. Wen, X. Wang, X. Zhang, D. Wang, X. Li, J. Loos, H. Chen, K. Walton and G. Marchand, *Polymer*, 2011, **52**, 5221-5230
12 S. Li and R. A. Register, *Macromolecules*, 2012, **45**, 5773-5781
13 F. Zuo, C. Burger, X. Chen, Y. Mao and B. Hsiao, *Macromolecules,* 2010, **43**, 1922–1929
14 J. Jin, C. Zhao, J. Du and C. C. Han, *Macromolecules* 2011, **44**, 4326–4334
15 T. Wen, G. Liu, Y. Zhou, X. Zhang, F. Wang, H. Chen, J. Loos and D. Wang, *Macromolecules*, 2012, **45**, 5979- 5985
16 J. Jin, J. Du, H. Chen and C. C. Han, *Polymer,* 2011, **52**, 6161-617 2
17 T. Wen, Y. Zhou, G. Liu, F. Wang, X. Zhang, D. Wang, H. Chen, K. Walton, G. Marchand and J. Loos, *Polymer*, 2012, **53**, 529-535
18 G. Liu, X. Zhang, Y. Liu, X. Li, H. Chen, K. Walton, G. Marchand and D. Wang, *Polymer,* 2013, **54**, 1440-1447
19 A.R. Kamdar, R.K. Ayyer, B.C. Poon, G.R. Marchand, A. Hiltner and E. Baer, *Polymer*, 2009, **50**, 3319–3328
20 Y. Lin, G. R. Marchand, A. Hiltner and E. Baer, *Polymer*, 2011, **52**, 1635-1644
21 P. Dias, Y.J. Lin, B. Poon, H.Y. Chen, A. Hiltner and E. Baer, *Polymer,* 2008, **49**, 2937-2946

22 J. Jin, H. Chen, M. Muthukumar and C. C. Han, *Polymer*, 2013, **54**, 4010- 4016
23 G. S. Shibulal and K. Naskar, *Express. Polym. Lett.,* 2012, **6**, 329-344
24 S. Wu, H. Li , G. Huang and J. Wu, *RSC Adv*. ,2014, 4, 19024-19033
25 Z. Z. Tong, B. Zhou, J. Huan g, J. T. Xu and Z. Q. Fan, *RSC Adv.* ,2014, **4**,15678- 15688
26Z. Z. Tong, B. Zhou, J. Huan g, J. T. Xu and Z. Q. Fan, *Compos. Sci. Technol*. 2013, **85**, 111 – 117
27 M. A. Manchado, J. Biagitti and J. M. Kenny, *Polym. Compos.* , 2002, **23**, 779-789
28 I. Choi and D. G. Lee, *Compos. Part A*, 2013, **48**, 1-8
29 A. Kalapakdee and T. Amornsakchai, *Polym. Test.* , 2014, **37**, 36-44
30 C. Hintze,R. Stocek, T. Horst, R. Jurk, S. Wiessner and G. Heinrich, *Polym. Eng. Sci.* , 2014, DOI: 10.1002/pen.23854.
31 J. Gao, Y. Dai, X. Wang, J. Huang, J. Yao, J. Yang, X. Liu, *Appl, Surf. Sci.* , 2013, **270**, 627-633.
32 A. Chantaratcharoen, C. Sirisinha1, T. Amornsakchai1, S. Bualek-Limcharoen1, and W. Meesiri, *J. Appl. Polym. Sci.* , 1999, **10**, 2414-2422
33 S. Zhao, L. Cheng, Y. Guo, Y. Zheng and B Li, *Mater Design*. , 2012, **35**, 749-753
34 Y.A. El-Shekeil, S.M. Sapuan, K. Abdan and E.S. Zainudin, *Mater Design.* , 2012, **40**, 299-303
35Z. Dong, M. Liu, D. Jia and Y. Zhou, *Chinese J. Polym. Sci.* , 2013, **31**, 1127-1138
36 M. Abdelmouleh, S. Boufi, M.N. Belgacem and A. Dufresne, *Compos. Sci. Technol*. 2007, **67**, 1627-1639
37 S. Jiang, A. Greiner and S. Agarwal, *Compos. Sci. Technol.* 2013, **87**, 164-169
38 S.M. Sapuan, H.Y. Lok, M.R. Ishak and S. Misri, Chinese *J. Polym. Sci.* , 2013, **10**, 1394-1403
39 G.S. Shibulal and K. Naskar, *Polym. Compos.* , 2013, DOI: 10.1002/pc.22830
40 G. Liu, X. Zhang, X. Li, H. Chen, K. Walton and D. Wang, *J. Appl. Polym. Sci.* , 2012, **125,** 666-675
41 G. Liu, X. Zhang, X. Li, H. Chen, K. Walton and D. Wang, *J. Appl. Polym. Sci.* , 2011, **119,** 3591-3597
42 R. S u, Z. Li, H. Bai, K. Wang, Q. Zhang, Q. Fu, Z. Zhang, and Y. Men, *Polymer*, 2011, **52**, 3655-3660
43 B. Na, K. Wang, P. Zhao, Q. Zhang, R. Du, Q. Fu, Z. Yu and E. Chen, *Polymer,* 2005, **46**, 5258-5267.
44 R. Su, K. Jiang, Y. Ge, S. Hu, Z. Li, X. Li, K. Wang, Q. Zhang, Q. Fu and F. Yang, *Polym. Int.* , 2011, **60**, 1655 -1662
45 J. Wang, Q. Mao and J. Chen, *J. Appl. Polym. Sci*. , 2013, **130**, 2176-2183
46 N. M. Barkoula and T. Peijs, *Polym. Compos.* ,2005, 26, 114-120
47Jiping Ye,T. Hasegawa and A. Suzuki. *J. Appl. Polym. Sci*. 2006, 100, 1306-1311
48 V. Caldas, G.R.Brown, R. S. Nohr and J. G. Macdonald. *J. Polym. Sci. Part B:Polym. Phys*. 1996 ,34, 2085-2098
49 T.N. Abraham, S.D. Wanjale, T. Bárány and J. Karger-Kocsis, *Compos. Part A,* 2009, **40**, 662-668
50 N. Ning, S. Fu, W. Zhang, F. Chen, K. Wang, H. Deng, Q. Zhang and Q. Fu, *Prog. Polym. Sci.* , 2012, **37**, 1425-1455
51M. Zhou, J. Yan, Y. Li, C. Geng , C. He , K. Wang and Q. Fu, *RSC Adv*. , 2013, **3** , 26418-26426
52 C. K. MOON, J. Appl. Polym. Sci. , 1998, 67, 1191-1197
53 S. Ju, Y. Wang, G. Huang and J. Chang, *RSC Adv*, 2013, 3, 8298-8307
54 E. Białecka-Florjańczyk. J. Phys. Chem. B, 2006, 110, 2582-2592
55 M. Khayet, G. Chowdhury and T. Matsuura. *AIChE Journal*, 2002, 48, 3833-3843
56 C. Han and S. Chun, *Macromolecules*, 1998, 31, 394-402
57 Z. Horvath, B. Gyar mati， A. Menyhard and P. Doshev, *RSC Adv*. ,2014, 4,19737-*19745*
58 M. Bailly and M. Kontopoulou. *Polymer* 50 (2009) 2472–2480
59 Y. Tang and M. Lewin, *Polym. Adv. Technol.*, 2009, 20, 1-15
60 R. Su, K. Wang, Q. Zhang, F. Chen and Q. Fu, *J. Phys. Chem. B* , 2009, **113**, 7423-7429